Lab on a Chip

Accepted Manuscript

ROYAL SOCIETY OF CHEMISTRY

www.rsc.org/loc

Cite this: DOI: 10.1039/c0xx00000x

www.rsc.org/xxxxxx

ARTICLE TYPE

Design and Characterization of Single Channel Two-Liquid Capacitor and its Application to Hyperelastic Strain Sensing

Shanlingzi Liu,[a] Xiaoda Sun,[a] Owen J. Hildreth,[a] and Konrad Rykaczewski*[a]

Received (in XXX, XXX) Xth XXXXXXXXX 20XX, Accepted Xth XXXXXXXXX 20XX

DOI: 10.1039/b000000x

Room temperature liquid-metal microfluidic devices are attractive systems for hyperelastic strain sensing. These liquid-phase electronics are intrinsically soft and retain their functionality even when stretched to several times their original length. Currently two types of liquid metal-based strain sensors exist for in-plane measurements: single microchannel resistive and two-microchannel capacitive devices. With winding serpentine channel geometry, these sensors typically have a footprint of about a square centimeter. This large footprint limits the areal density that the devices that can be embedded into a wearable electronic skin. In this work we introduce an alternative capacitor design consisting of two liquid metal electrodes separated by a liquid dielectric within a single straight channel. Using a liquid insulator instead of a solid elastomer enables us to tailor the system's capacitance by selecting high or low dielectric constant liquids. We quantify the effects of the electrode geometry including diameter, spacing, and meniscus shape as well as dielectric constant of the insulating liquid on the overall system's capacitance. We also develop a procedure for fabricating the two-liquid capacitor within a single straight Polydiemethylsiloxane channel and demonstrate that this device can have about 25 times higher capacitance per sensor's base area when compared to two-channel liquid metal capacitors. Lastly, we characterize response of this compact device to strain and identify operational issues arising from complex hydrodynamics near liquid-liquid and liquid-elastomer interfaces.

1. Introduction

Stretchable electronic components have applications in flexible electronics, biomedical devices, and soft robotics.[1-4] Room-temperature liquid metals are attractive materials for fabrication of such devices because they retain their functionality even when stretched to several times their original length.[5] Whitney strain gauge developed in late 1940's is the earliest example of liquid metal electronics.[6] This device measures strain of a mercury-filled rubber tube by measuring change in electric resistance of the metal. While in the last two decades mercury and rubber have been replaced by non-toxic liquid gallium alloys (i.e. GaIn and GaInSn) and more elastic Polydiemethylsiloxane (PDMS), the resistive design of the liquid metal strain sensor remains popular. One of the limitations of the resistive devices is that their large footprint limits the areal density that they can be embedded into a wearable electronic skin. For example a ~1 Ω resistor made out of GaInSn with resistivity of 0.29 μΩm in a 200 μm diameter channel has a length of ~10 cm. By winding the channel 10 times such sensor can be fit into an area of ~1 cm^2. Improved understanding of the GaIn and GaInSn wetting characteristics[7-13] and advances in their micro-fabrication[4, 14-25] are enabling fabrication of smaller liquid metal filled microchannels with higher areal density; however, the required serpentine geometry of these resistors remains quite complex. Several designs of capacitive strain sensors have been proposed as alternatives to the resistive devices.[26, 27] These capacitive devices consist of two microchannels filled with liquid metal separated by the dielectric PDMS matrix (see schematic in Fig.1a). For in-plane sensing an order of magnitude estimate for the required sensor footprint can be obtained using the parallel plate capacitor model, $C \approx \varepsilon_0 \varepsilon A / d$ (i.e. $A \approx Cd/\varepsilon_0\varepsilon$). To achieve a capacitance (C) of ~1 pF, two liquid metal-filled microchannels with both height (h) and separation (d) of ~400 μm within a PDMS matrix (ε~2) must have a length of l~10 cm (from conductor-dielectric interfacial area, $A \sim lh \sim 4\text{x}10^{-5}$ m^2). By winding the parallel channels in a serpentine arrangement, such a sensor can fit within a base area of several square centimeters. Fassel and Majidi[27] recently showed that such base area is required for a variety of winding two-channel capacitive strain sensor designs to achieve C~1-15 pF. With such a large footprint the sensor output is affected by stretching in multiple directions, not only in the desired principle direction. As a result, correlation of the physical strain with the sensor output is complex.[27]

Since parallel plate capacitance is proportional to both the conductor-dielectric interfacial area and the dielectric constant, a decrease in the required length of the parallel channels, and with that the sensor footprint, should be achievable by increasing the dielectric constant of the insulator material. While solid elastomers with ε greater than that of PDMS (ε~2) are not readily available, common liquids like glycerol and water have ε~40 and

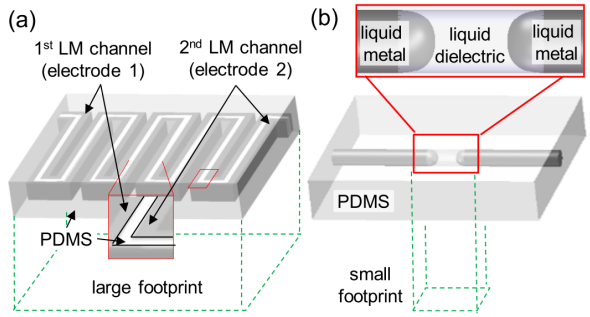

Fig. 1 Schematic comparison of capacitor geometries comprising of (a) two winding liquid metal filled channels separated by solid elastomer and (b) single channel filled with liquid metal and liquid dielectric.

ε~80, respectively. According to the parallel plate model scaling, replacing PDMS with these dielectric liquids would decrease the required conductor-dielectric interfacial area of a sensor by 20 to 40 times.

Motivated by these simple scaling arguments we explore the concept of a capacitor composed of two liquid metal electrodes separated by a liquid dielectric within a single straight cylindrical microchannel (see schematic in Fig.1b). We use simulations and an experimental setup consisting of two GaInSn filled tubes submerged within a dielectric liquid bath to quantify the effects of the cylindrical electrode geometry including diameter, spacing, and meniscus shape as well as dielectric constant of the insulating liquid and the presence of tubing on the overall system's capacitance. Next, we describe a procedure for fabricating the two-liquid capacitor within a single straight cylindrical PDMS channel. We characterize capacitance and response of this compact device to strain and identify operational issues arising from complex hydrodynamics near liquid-liquid and liquid-elastomer interfaces.

2. Results and Discussion

2.1 Effects of Geometry and Dielectric Liquid on Capacitance of the Two-Liquid System

In order to systematically study the effects of geometry on capacitance of the two-liquid system without the hassle of fabrication of multiple devices we have developed a simple testing setup shown in Fig. 2a (see also Fig.S2). This system consists of two GaInSn filled thin-walled PVC tubes (ε~3.2) that are aligned along the same axis and submerged in a dielectric liquid bath. The tubes were filled with GaInSn up to their open ends, which were arranged to face each other. The separation distance between the two tubes was adjusted using a micrometer and the shape of the each of the liquid metal-liquid dielectric interfaces was controlled by applying pressure to the syringes that were used to supply the liquid metal. We also numerically simulated the capacitance of the various systems with 2D axisymmetric geometry using COMSOL Multiphysics 5.0 modelling software. Example potential fields around flat-ended cylinders with and without tubing as well as parallel plates with and without electric fringe effects are shown in Fig.2b. We note that due to high solubility of oxygen in glycerol and water as well as its high permeability through PDMS[12, 14] a ~2 nm thick gallium oxide skin is likely to form at the two liquid interface. However, its presence will have negligible effect on the system's capacitance.†† Further details of the setup fabrication are described in the Experimental Section and those of of the numerical simulation in Support Information, while experimental and simulation results are described below.

2.1.1 Effects of separation distance and dielectric liquid

We first measured capacitance of two flat-ended cylindrical electrodes with diameters of 1 mm and 2 mm separated by 0.1 mm to 13.5 mm that were submerged within glycerol, water, and as reference, silicone oil. The latter insulator has a dielectric constant between 2.2 to 2.8 and served as a control to mimic the PDMS elastomer. The plots in Fig. 2c and 2d show that by replacing silicone oil with glycerol and water the system's capacitance increases from ~1-1.5 pF to ~4-5 pF and ~6-7 pF for electrode separation distances below ~0.5 mm, respectively. This 3 to 5 fold capacitance increase is significantly smaller than the ~15 (40/2.8) to ~30 (80/2.8) increase predicted by dielectric constant ratios described in introduction section. In addition, doubling of the electrode diameter increases the measured capacitance by a factor of two not four as predicted by the basic parallel plate model. To explain these trends we compared experimental data to simulations as well as theoretical predictions using the parallel plate model with and without fringe effects. The latter model derived by Landau et al. [28] takes into account that electrical field does not end abruptly outside of the electrode plates, and incorporates the electrical field fringe effects illustrated in Fig. 2b around the edges of the two electrodes (but not along the cylinder):

$$C = \varepsilon_0\varepsilon\left[\left(\frac{\pi r^2}{d}\right) + r ln\left(\frac{16\pi r}{d} - 1\right)\right] \qquad \text{Eq. 1}$$

where r is the electrode radius. The plot in Fig.2e compares typical measured capacitance (in this case 1 mm diameter electrodes wrapped in 0.5 mm thick tubing separated by glycerol) as function of separation distance to the simulation and analytical predictions. For small separation distances, the experimentally measured capacitance decreased proportionally to $1/d$, in agreement with the parallel plate model scaling. However, when the separation distance was greater than ~1 mm, the measured capacitance values exceeded those predicted by either of the models by two to three times. In contrast, the simulation results, which capture the effects of electrical field along the cylinders as well as presence of the tube and the dielectric liquid outside the separation gap match the experimental data well (see Fig.S3a and S3b for more simulation results). The simulations results in Fig.2f also show that the addition of tubing around the liquid metal electrodes results in a large decrease of the system's capacitance. Without the tubing, switch from silicone oil to glycerol and water for 1 mm ID cylinders separated by 10 mm increases the capacitance from 0.37 pF to 3.93 pF and 7.76 pF, respectively. This corresponds to a ~11 and ~21 fold capacitance increase related to the dielectric liquid change. The ~30% discrepancies between these values and those predicted from dielectric constant scaling likely stem from the finite dielectric bath volume in simulations, which were designed to represent our experimental "bath" system. The presence of tubing, however, does not account for the capacitance scaling with radius of the cylinders, not their end-areas. In particular, according to simulations,

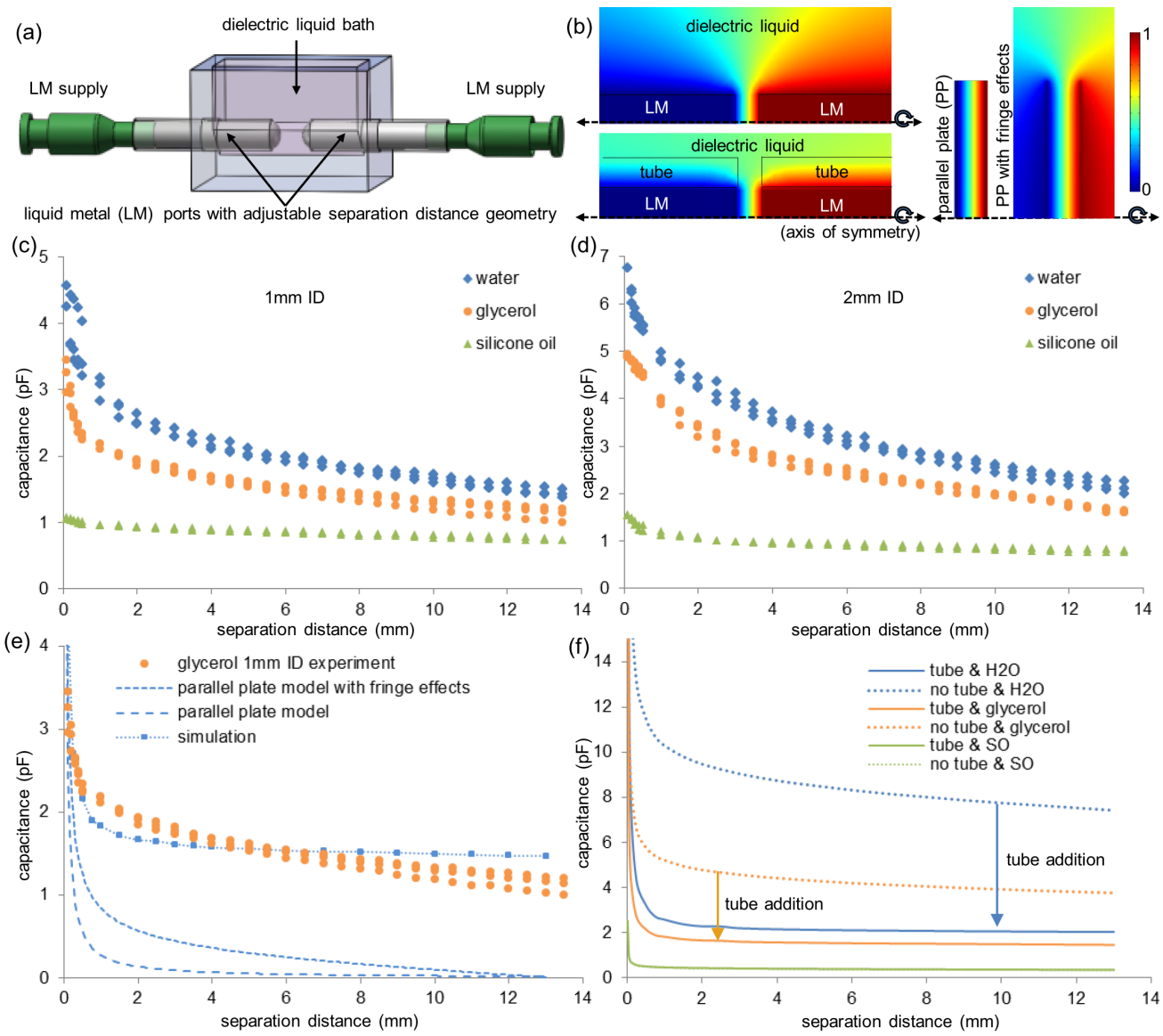

Fig.2 (a) Schematic of the setup used to characterize the capacitance of the liquid metal (LM)-liquid dielectric capacitor, (b) example simulated potential fields around capacitors consisting of flat-ended cylinders with and without tubing as well as parallel plates with and without electric fringe effects, (c-d) measured capacitance of two flat-ended cylindrical metal electrodes with diameter of (c) 1 mm and (d) 2 mm separated by silicone oil, glycerol, and water, (e) comparison of experimentally measured, simulated, and calculated capacitance using parallel plate model with and without fringe effects for two flat-ended cylindrical metal electrodes with 1 mm diameter separated by glycerol, and (f) comparison of simulated capacitance values for cylinders with and without tubing.

increase of two "tube-less" metal cylinder diameters separated by 10 mm from 1 mm to 2 mm in silicone oil, glycerol, and water increases the capacitance by ~2.2 (7.9/3.7), ~2.5 (8.6/3.4), and ~2.2 (16.9/7.8), respectively. This confirms strong influence of the electric field fringe effects along the tube as well as outside the electrode separation area, the latter of which scale with the radius of the electrode according to Eq. 1.

2.1.2 Effect of Liquid-Liquid Interface Shape

Next we investigated how curvature of the liquid metal-liquid dielectric interfaces affects the system's capacitance. Quantification of this effect is particularly relevant for the two-liquid capacitor because a meniscus is likely to form at the liquids' interface due to the large difference between their surface tensions.[14] We measured capacitance of electrodes with two types of menisci shown in Fig.3a. The geometry of the menisci approached that of spherical-caps with liquid metal-tube contact angles (θ) of ~55-60° and ~90-100°, as defined from the line connecting the edges of the tube. We also simulated the capacitance of the two-electrode system with θ=90° (see Fig. 3b).We report the results in Fig.3c and 3d in terms of meniscus-tip to meniscus-tip separation distance, while data in terms of meniscus base-to-meniscus base (i.e. end-of-tube to end- of-tube) separation distance is provided in Support Information. We decreased the tip-to-tip distance until the electrodes touched and short-circuited by merging. Plots in Fig.3c to 3d show that highest capacitance was measured for the systems consisting of two electrodes with menisci with θ~90-100° (i.e. about hemispherical), irrelevant of how the separation distance was

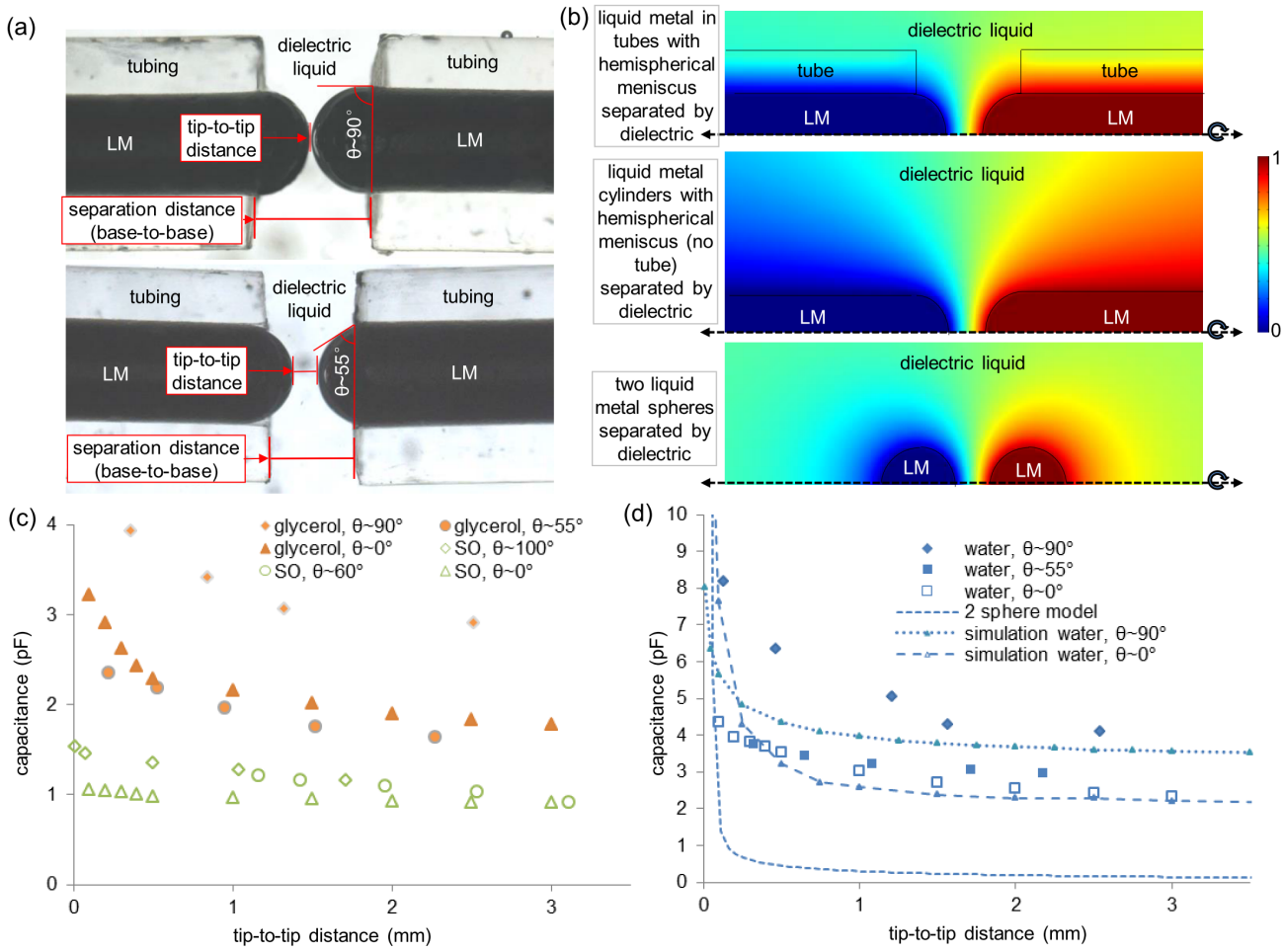

Fig.3 (a) Example images of two-liquid capacitors with meniscus-ended electrodes with θ~60° and θ~90°, (b) example simulated potential fields around capacitors consisting of hemisphere-ended cylinders with and without tubing as well as two spheres, (b-d) plots of measured capacitance of two symmetrical meniscus-ended electrodes separated by (b) glycerol and silicone oil, (c-d) water as function of (b-c) separation distances (base-to-base) and (d) tip-to-tip separation distances defined in (a).

specified. To theoretically take into account the meniscus shape, we also compare the experimental data in Fig. 3d to both simulations and series solution predicting capacitance of two conducting spheres. The analytical solution to this problem was first derived by Maxwell using method of images[29] and recently solved using bispherical coordinates by Gongora and Ley-Koo:[30]

$$C = 4\pi\varepsilon_0\varepsilon\frac{a}{2}\sum_{l=0}^{\infty}\left(l+\frac{1}{2}\right)C_l(cosh\eta_1)C_l(cosh\eta_2)\text{csch}\left[\left(l+\frac{1}{2}\right)(\eta_1-\eta_2)\right] \quad \text{Eq. 2}$$

In Eq. 2 the two spheres are positioned along z-coordinate are defined by a and η_i in the bi-spherical system with $r_i = a|cschn_i|$ and $z_i = acothn_i$. The function $C_l(cosh\eta_1)$ is defined as:

$$C_l(cosh\eta_1) = \frac{1}{2^l N_l}(sech\eta_1)^{\frac{1}{2}+l}\ {}_2F_1\left(\frac{l}{2}+\frac{1}{4},\frac{l}{2}+\frac{3}{4},l+\frac{3}{2},sech^2\eta_1\right) \quad \text{Eq.3}$$

In Eq.3 N_l are normalization factors of the Legendre polynomials ($N_0 = 1, N_1 = 1, N_2 = 0.5, N_3 = 0.5, N_4 = 0.125, N_5 = 0.125$ etc.) and ${}_2F_1$ is the hypergeometric function. Unfortunately, as shown in Fig.3b, the two-sphere model does not capture well the potential field distribution outside of the two-electrode separation gap and along the cylinders (with and without tubing). Consequently, the analytical model significantly under predicts the capacitance. However, as in the case of flat-ended cylinders, the simulated values match the experimental values reasonably well (see Fig. 3d). As observed in the experiments, the simulated capacitance of the hemisphere-ended cylinder system exceeds that of flat-ended cylinder system for separation distances greater than ~0.1 mm. This effect likely stems from combination of the electric field distribution and larger interfacial "cap" area of the hemisphere ($2\pi r^2$ vs. πr^2).

2.2 Single Channel Two-Liquid Capacitive Strain Sensor

2.2.1 Device Fabrication Procedure

The results presented in Section 2.1 show that a two-liquid capacitor can have C~5-8 pF with a footprint of only 1-2 mm^2 (i.e. ~50 fold reduction comparing to two channel capacitors). Motivated by these results, in this Section we explore viability of a single-channel two-liquid capacitive strain sensor. This device differs from the experimental setup used in Section 2.1 in that the liquid metal electrodes and the liquid dielectric are encapsulated within a single channel as oppose to having two liquid metal filled tubes separated by a liquid dielectric bath. As shown in

schematic in Fig.4, the device was fabricated by casting elastomer solution over a 3D printed rectangular casing pierced by a horizontal stainless steel shaft. After thermal curing of the elastomer, we created the two-open ended cylindrical channel by removing the casted elastomer from the mold and pulling out the steel shaft. Filling of this channel with liquid metal electrodes separated by the liquid dielectric was the primary challenge in fabricating the two-liquid capacitive strain sensor. In principle this could be achieved by altering flow of the two liquids. However, flowing of silicone oil, glycerol, and water into the PDMS channel filled with GaInSn resulted in residual liquid metal patches adhering to the channel walls (see Fig. 4c). In general, this can be attributed to the formation and resulting morphology of the gallium oxide shell-substrate interface.[12] To resolve this issue we "lubricated" the PDMS channel prior to flowing GaInSn with flow of the dielectric liquid, preventing residual GaInSn adhesion to the PDMS walls. This observation was also recently reported by the Dickey group.[31] After lubricating the channel with the dielectric, we injected liquid metal via a small temporary vertical hole near the middle of the channel. Temporarily sealing of one of the channel ends enabled the liquid metal to push out about half of the dielectric liquid out

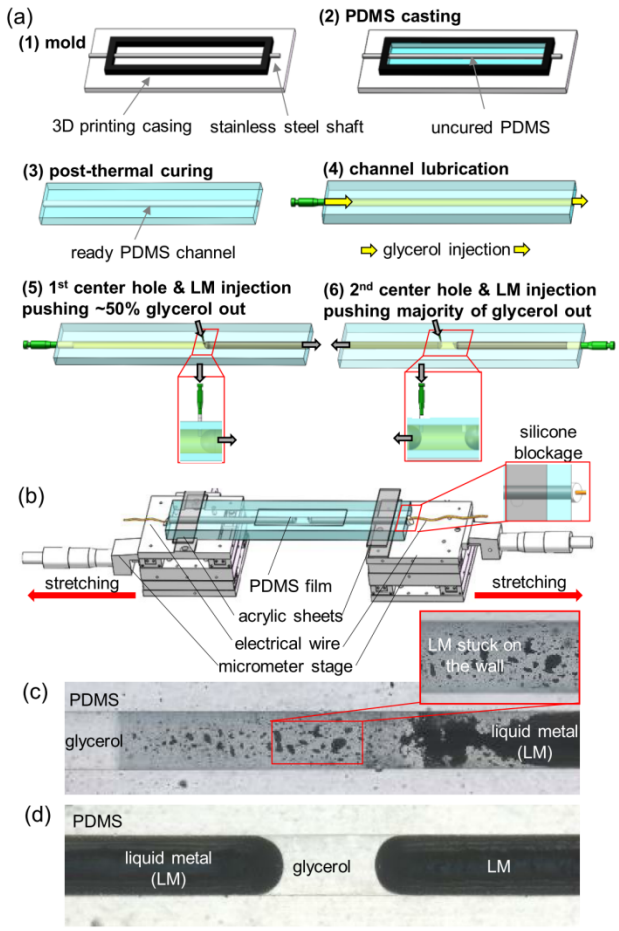

Fig.4 (a) Schematic of the single channel two-liquid capacitor fabrication procedure and its mounting in the (b) strain testing setup; (c) image showing residual liquid metal (LM) after it was partially pushed out with glycerol flow, (d) image of fabricated 1.6 mm diameter two-liquid capacitor fabricated using procedure shown in (a).

of the channel through the open-end. After sealing of the first vertical hole with PDMS, majority of the remaining liquid dielectric was pushed out through the previously sealed end by liquid metal that was injected through a second temporary vertical hole made nearby the original one. The image in Fig.4d shows that this procedure avoids sticking of liquid metal to the walls and can be used to fabricate single channel GaInSn-glycerol-GaInSn and GaInSn-water-GaInSn junctions. Since the surface tension of glycerol (63 mN/m) and water (72 mN/m) is much smaller than that of GaInSn (718 mN/m), the liquid metal forms a convex or "bulging" hemispherical meniscus on both sides of the junctions.

2.2.2 Device performance

The described procedure could be used to repeatedly fabricate single channel two-liquid capacitors with glycerol and water as dielectric liquids. However, fabrication of a complete two-liquid device that was stable in "static" conditions did not guarantee its stability during stretching. For example, the image in Fig.5a shows that during initial stages of stretching of the GaInSn-water-GaInSn capacitor, the liquid metal electrodes did not move gradually, but "snapped" leaving behind residue on the PDMS walls. The sudden movement and residual GaInSn indicate that the oxide shell grew at the liquid metal-PDMS interface causing the high adhesion. Consequently, we found use of water as dielectric liquid to be impractical, and focused on capacitors filled with glycerol.

Due to the manual nature of the current fabrication process the electrode-to-electrode separation distance was difficult to control. The minimal menisci tip-to-tip distance that we were able to fabricate using this procedure was ~2.3 mm. This system had an unstrained capacitance (C_0) of 1.1 pF with a footprint of about 3 mm^2. We observed that the separation distance between the two electrodes can be reduced by compressing the other edges of the PDMS channels filled with liquid metal. This forced some of the glycerol stored in-between the electrodes to flow into the thin annular gap along the PDMS and GaInSn interface. Using this approach we were able to reduce the tip-to-tip electrode separation distance down to ~0.5 mm to ~1 mm, which produced capacitance of ~2 pF to ~1.4 pF with a corresponding footprint of ~0.8 mm^2 to 1.6 mm^2.

We measured the capacitance of several glycerol-liquid metal capacitors channels during stretching using the setup illustrated in Fig.4b. The plot in Fig.5b shows the response to strain of devices that had as-fabricated electrode separation distance (s5 to s7) as well as several devices that had the electrode-separation distance reduced by compressing the outer edges of the PDMS channels (s1 to s4). All the devices had initial tip-to-tip separation distance in the range of ~0.5 mm to ~2.5 mm. Since the devices had different initial electrode-to-electrode spacing, the data is presented in absolute terms. While all the data follows the trends expected from Fig. 2 and 3 as well as simulation of the system, the geometry of devices was by the stretching process in two ways. The first mode involved separation of the liquid metal electrode induced by the device stretching. The plot in Fig. 5c shows stretching data for the "s2" device with corresponding images of the electrodes prior to and at the end of stretching. One of the electrodes in this device was separated into two parts through gradual necking as

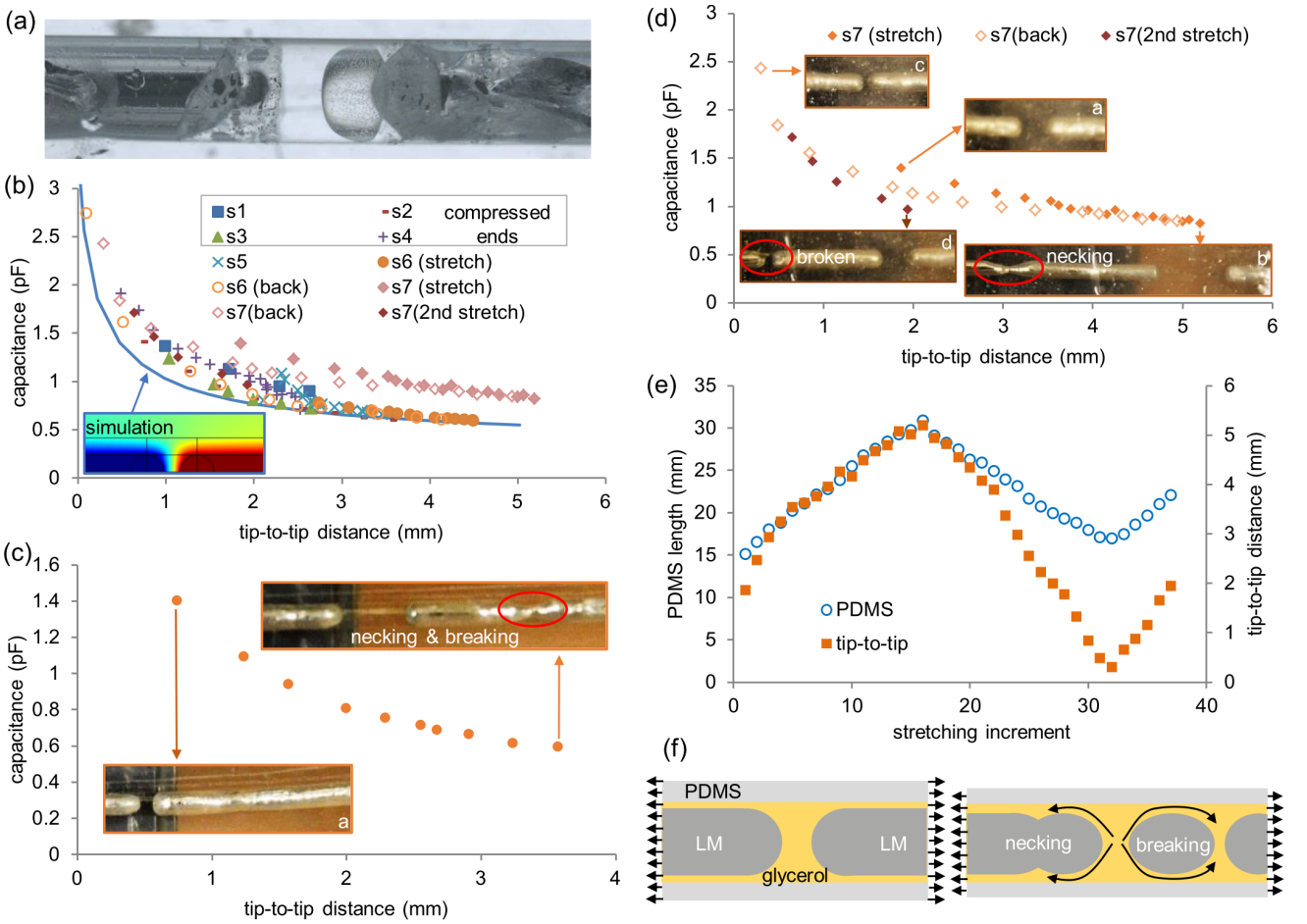

Fig.5 (a) Image of GaInSn-water-GaInSn device after initial stretching, (b-d) plots of measured capacitance as function of liquid metal menisci tip-to-tip separation distance for various GaInSn-glycerol-GaInSn devices: (b) all devices, (c) s2 device which had electrode separation distance reduced by "squeezing" or "compressing" the non-facing device ends, (d) s7 device whose non-facing device ends were not compressed, (e) comparison of PDMS device length and electrode menisci tip-to-tip separation distance during stretching, and (f) schematic of the glycerol device failure modes induced by glycerol outflow into the annual region separating PDMS and the electrodes.

the device was stretched. Separation of the two electrodes created two capacitors in series, which significantly decreased the total capacitance. The role of the glycerol outflow from the electrode separation region is clearly highlighted in the second scenario illustrated in Fig.5d and 5e. Specifically, neither of the electrodes separated as the menisci tip-to-tip distance was increased from ~2 mm to ~5 mm (stretch ratio of 5/2~2.5). Plot in Fig. 5e shows that during this part of stretching the PDMS length and the menisci tip-to-tip distance were roughly proportional, with a stretch ratio of ~2 observed for PDMS. However, during the retraction the two distances did not decrease proportionally. In particular, the separation distance between the electrodes decreased below the starting ~2 mm to ~0.1 mm. Naturally, for this to occur the glycerol must have been displaced by the liquid metal. The decrease of the electrode distance increased the capacitance to ~2.5 pF from the starting C_0 ~1.4 pF. For this device, glycerol outflow to the annual region only caused necking during the first stretching and retraction (back) cycle. The images in Fig.5e show that the one of the electrodes finally separated during the second stretching cycle. We schematically show in Fig.5f that both the electrode necking and breaking are due to glycerol outflow into the annual region between the electrode and PDMS. Once excess glycerol is stored within this region, stretching of the device induces radial stresses which force the glycerol to break up the liquid metal electrode.

3. Conclusions

In this work we introduced a novel concept for a capacitor consisting of a liquid dielectric sandwiched in-between two liquid metal electrodes within a single straight cylindrical channel. In the first part of this paper, we used simulations and a simple setup consisting of two liquid metal filled tubes submerged in dielectric liquid bath to quantify the effects of the electrode geometry including diameter, separation distance, and menisci shape as well as dielectric constant of the insulator liquid on the system's capacitance. We demonstrated that by replacing silicone oil with glycerol and water a three to five fold increase in the system's capacitance can be achieved. This increase is substantial but not as large expected based on the ratio of the dielectric constants of the insulator liquids. Using simulations we showed that this effect is due to the presence of low dielectric constant tubing (PVC and

PDMS). Using simulations we also demonstrated that electric fringe effects outside the separation gap and along the cylinder are responsible for the capacitance scaling with radius of the electrodes not its square. We found that for all geometries the measured capacitance cannot be predicted by classical analytical models for parallel plate or two-spheres capacitors and that full system numerical simulation is required to adequately capture the electrical field distribution. With optimal geometry comprised of hemispherical menisci and minimal separation distance, we found that glycerol and water systems with capacitance of ~5 pF to ~8 pF and a footprint of only ~1-2 mm^2 are feasible.

In the second part of this paper, we explored feasibility of using a two-liquid capacitor within a single PDMS channel for hyperelastic strain sensing. Residual GaInSn adhesion to the channel walls was prevented by lubricating the PDMS channel with water and glycerol prior to liquid metal injection. This enabled fabrication of single-channel liquid metal capacitors separated by glycerol and water. Unfortunately, oxide regrowth at the GaInSn-PDMS interface in presence of water rendered strain sensors with water as dielectric material impractical. In particular, when stretching, the liquid metal electrodes did not deform gradually, but suddenly "snapped" leaving behind residual GaInSn on the PDMS walls. This behavior was not observed in glycerol devices, indicating persistent PDMS wall lubrication by this dielectric liquid. For glycerol devices fit within a 1.6 mm diameter channel, the minimal menisci tip-to-tip distance that we achieved with and without compressing of the device's outer edges was ~0.5 mm and ~2.3 mm, corresponding to capacitance of ~2 pF and ~1.1 pF with footprint of ~0.8 mm^2 and ~3 mm^2, respectively. Thus, we demonstrated that a single PDMS channel two-liquid capacitor can have about a ~25 fold higher capacitance per sensor base area as compared to current winding two-channel capacitors (2 pF/0.8 mm^2 vs. ~10 pF/100 mm^2). However, further experiments revealed that the liquid metal electrode geometry was altered by stretching. In particular, pressure induced by the stretching caused outflow of glycerol from the region separating the electrodes to the annual region between the electrode and the PDMS channel wall. As a result, necking and breaking of the liquid metal electrodes was observed. Thus, while enabling fabrication and facile movement of the liquid metal electrodes, the presence of the "lubricating" glycerol also causes failure of the two-liquid capacitor.

Our work illustrates that single channel two-liquid capacitors could provide a ~25 times more compact alternative to current capacitive liquid metal strain sensors. However, application of the two-liquid capacitor to strain sensing is limited by glycerol-liquid metal fluid dynamics induced by stretching. We note that this does not represent a fundamental barrier, rather a problem that could be resolved by an alternative fabrication procedure or altered design. Possible alternative designs could include modification of the channel wall surface to reduce GaInSn adhesion,[12, 13, 32, 33] alternative channel filling procedure[34] or hybrid approach between the single channel design and multichannel design recently introduced by Ota et al.[35] Another possibility is to include an "overflow" region for the glycerol squeezed out of the center region.

4. Experimental Section

Materials

GaInSn with the composition of 68.5% Ga, 21.5% In, and 10% Sn was purchased from Rotometals. Water was purified to a resistivity of 18 MΩ-cm using Thermo Scientific™ Barnstead™ NanoPure™ system. Glycerol (≥99.5%, Sigma-Aldrich G9012) and silicone oil (viscosity 100cSt, Sigma-Aldrich, 378364) were used as the other two dielectric liquids. Elastomer substrates for capacitive strain sensors were fabricated by mixing elastomer base weighing 10 parts (around 15 g) and curing agent weighing 1 part (around 1.5 g) (Dow Corning, Sylguard 182, silicone elastomer kit).

Two liquid metal filled tube within dielectric bath setup

The ABS system housing was 3D printed using Makerbot Replicator 2X and filled with the dielectric liquids. The housing had two ports for passing liquid metal channels made of 1mm or 2mm internal diameter (ID) Masterkleer PVC tubing (Mcmaster-Carr), which was connected to 1 mL plastic syringes (Mcmaster-Carr) with corresponding 0.08 cm or 0.2 mm ID and 1.26 cm length blunt tip dispensing needles (Mcmaster-Carr). The spacing between the ends of the liquid metal tubes was adjusted using two micro-positioning stages (Deltron, 1201-XYZ) attached to the 3D printed syringe holders using adhesive tape. For all of the tests, we used 889B Bench LCR/ESR Meter to measure capacitance and dissipation factors at frequency of 200 kHz and voltage of 1V in parallel mode. A home-made faraday cage was used to shield the devices from electromagnetic interference during measurements. To make electrical contacts, copper wires were soldered onto the conductive syringe needles. The stray capacitance of the system was quantified with just air at different levels of relative humidity as well as long electrode separation distances. The results presented in Fig. S4c-e show that the stray capacitance was negligible.

To study the effect of the liquid metal meniscus shape on device capacitance, the bottom of the 3D printed housing was replaced by pre-cleaned glass slide (Thermo Scientific). This modification enabled detailed visualization of the meniscus shape using transmitted light in Zeiss Axio-Zoom V 16 microscope fitted with a Z 1.5x/0 37 FWD 30mm lens. Menisci with two different spherical-cap shapes characterized by the metal-tube contact angles of ~60° and ~90° were fabricated by manually adjusting the syringes. The capacitance was measured off-site within the faraday cage after the geometry of the device was adjusted under the microscope.

Single channel two-liquid capacitor fabrication procedure

The channel was fabricated within a single step by casting the elastomer solution over a 3D printing rectangular casing pierced by a 1.6 mm diameter and 7.6 cm length stainless steel shaft (McMaster-Carr). The PDMS solution was mixed in petri dishes and poured into the mold. Before curing the PDMS mixture was degassed for around 30 minutes until all air bubbles escaped. Subsequently, the casted was heated for 1.5 h at 85°C on hot plate. After curing, the cast was removed from the mold, with the steel shaft simply pulled out to create the two open-ended channel with circular cross-section. To fabricate the three sandwiched liquids layout while preventing the liquid metal from adhering to the wall of the channel during stretching, we injected the dielectric liquids first in order to lubricate the channel. Next, we blocked one side of the channel with a syringe and injected

GaInSn by piercing a hole through the top of the PDMS into the channel using 1 mL syringe with 1.26 cm long 0.03 cm ID blunt tip dispensing needles (McMaster-Carr, 75165A686). As a result the insulating liquid was ejected from the free side of the channel. To prevent leakage during testing, we sealed the vertical hole with a few drops of the uncured elastomer to the hole on the top and let it cure naturally without additional heating (to prevent hardening of the PDMS). After the first hole was sealed, another point located a specified distance away from the first one was made and liquid metal was injected again to push out majority of the dielectric liquid from the channels. The result was a controlled amount of dielectric liquid separating the GaInSn. To finalize the device fabrication, wires were inserted into the ends of the channels.

PDMS sensor stretching experiments

The ends of the PDMS devices were mounted onto two micro-positioning stages (Deltron, 1201-XYZ) by sandwiching them between flat acrylic "clamps". For experiments involving the devices with "compressed" non-facing ends, the channel ends were fitted with a thin copper wire and sealed using silicone prior to mounting on the stage (thus clamping compressed the ends of the device). For testing of the not squeezed devices, the channel ends were sealed after clamping onto the stage. During each stretching step the device was photographed from top-down using Nikon 3200 camera. The capacitance of the system without the PDMS channel being filled with liquid metal electrodes (so wires, stages etc.) in air below 50% relative humidity was below 0.15 pF for PDMS with length of ~2.7 cm.

Acknowledgements

Konrad Rykaczewski acknowledges startup funding from Fulton Schools of Engineering at ASU. The authors acknowledge Mr. Viraj Damle from ASU and Prof. Kyle Doudrick from University of Notre Dame for their insightful comments

Received: ((will be filled in by the editorial staff))
Revised: ((will be filled in by the editorial staff))
Published online: ((will be filled in by the editorial staff))

Notes and references

[a] School for Engineering of Matter, Transport and Energy, Arizona State University, 501 E Tyler Mall, Tempe, AZ, 85287, US

*Email: konradr@asu.edu

† We note that while closed-form or series analytical solutions for capacitance for variety of geometries exist,[29, 30, 36] one matching our case even with flat-ended wires was not available in literature.

†† Capacitance of two parallel plates separated by multiple dielectrics materials can be estimated as $C = \varepsilon_0 A / \sum_i \varepsilon_i / d_i$.[37] Based on this relation the contribution of the oxide layers (on two interfaces) with $d \approx 2$ nm and $\varepsilon_{Ga2O3} \approx 10$ [38] is negligible to the two-liquid device capacitance. We note while typically the oxide skin growth is self-terminating, several authors have recently demonstrated that a thicker oxide skin can be grown electrochemically.[39, 40] However, this is not likely to be an issue in the case of the proposed device since an electrolyte, not dielectric liquid is used. Furthermore, even with the reported thickness of up to 5 nm the effect on the device capacitance is negligible.

Electronic Supplementary Information (ESI) available: [details of any supplementary information available should be included here]. See DOI: 10.1039/b000000x/

1.J. A. Rogers, T. Someya and Y. Huang, *Science*, 2010, **327**, 1603-1607.
2. D.-H. Kim and J. A. Rogers, *Adv. Mater.*, 2008, **20**, 4887-4892.
3. S. Cheng and Z. Wu, *Lab Chip*, 2010, **10**, 3227-3234.
4.J. Park, S. Wang, M. Li, C. Ahn, J. K. Hyun, D. S. Kim, J. A. Rogers, Y. Huang and S. Jeon, *Nat. Comm.*, 2012, **3**, 916.
5. S. Cheng and Z. Wu, *Lab Chip*, 2012, **12**, 2782-2791.
6.R. Whitney, *J. Physiology*, 1949, **109**, Proc, 5.
7.M. D. Dickey, R. C. Chiechi, R. J. Larsen, E. A. Weiss, D. A. Weitz and G. M. Whitesides, *Adv. Funct. Mater.*, 2008, **18**, 1097-1104.
8.R. C. Chiechi, E. A. Weiss, M. D. Dickey and G. M. Whitesides, *Angewandte Chemie*, 2008, **120**, 148-150.
9. D. Kim, P. Thissen, G. Viner, D.-W. Lee, W. Choi, Y. J. Chabal and J.-B. Lee, *ACS Appl. Mater. Interfaces*, 2013, **5**, 179-185.
10.T. Liu, P. Sen and C.-J. Kim, IEEE 23rd Int. Conf. on MEMS, 2010, 560-563.
11.T.Liu, P. Sen and C.J Kim, *J. MEMS*, 2012, **21**, 443-450.
12.K. Doudrick, S. Liu, K. L. Klein, E. M. Mutunga, K. K. Varanasi and K. Rykaczewski, *Langmuir*, 2014, **30**, 6867-6877.
13.R. K. Kramer, J. W. Boley, H. A. Stone, J. C. Weaver and R. J. Wood, *Langmuir*, 2014, **30**, 533-539.
14.J. Thelen, M. D. Dickey and T. Ward, *Lab Chip*, 2012, **12**, 3961-3967.
15.H. Yang, C. R. Lightner and L. Dong, *ACS Nano*, 2011, **6**, 622-628.
16.B. L. Cumby, G. J. Hayes, M. D. Dickey, R. S. Justice, C. E. Tabor and J. C. Heikenfeld, *App. Phys. Lett.*, 2012, **101**, 174102-174102-174105.
17. S. H. Jeong, A. Hagman, K. Hjort, M. Jobs, J. Sundqvist and Z. Wu, *Lab Chip*, 2012, **12**, 4657-4664.
18. A. Tabatabai, A. Fassler, C. Usiak and C. Majidi, *Langmuir*, 2013, **29**, 6194-6200.
19. J. Wissman, T. Lu and C. Majidi, *IEEE Sensors*, 2013, 1-4.
20.Y. Zheng, Q. Zhang and J. Liu, *Applied Physics A,* 2014, **116**, 1091-1097.
21. Y. Zheng, Z.-Z. He, J. Yang and J. Liu, *arXiv*, 2013, 1312.0617.
22. J. W. Boley, E. L. White, G. T. C. Chiu and R. K. Kramer, *Adv. Funct. Mater.*, 2014, **24**, 3501-3507.
23. R. K. Kramer, C. Majidi and R. J. Wood, *Adv. Funct. Mater.*, 2013, **25**,5929-5285.
24.C. Ladd, J.-H. So, J. Muth and M. D. Dickey, *Adv. Mater.*, 2013, **25**, 5081-5085.
25.B. A. Gozen, A. Tabatabai, O. B. Ozdoganlar and C. Majidi, *Adv. Mater.*, 2014, **26**, 5211-5216.
26.R. D. Ponce Wong, J. D. Posner and V. J. Santos, *Sens. Actuat. A*, 2012, **179**, 62-69.
27.A. Fassler and C. Majidi, *Smart Mater. Struct.*, 2013, **22**, 055023.
28. L. D. Landau, J. S. Bell, M. J. Kearsley, L. P. Pitaevskii, E. M. Lifshitz and J. B. Sykes, *Electrodynamics of Continuous Media.* , Elsevier, 1984.
29.J. C. Maxwell, *A Treatise on Electricity and magnetism*, Oxford, 3rd edn., 1892.
30.A. Gongora and E. Ley-Koo, *Rev. Mex. Fis.*, 1996, **42**, 663-667.
31.M. R. Khan, C. Trlica, J.-H. So, M. Valeri and M. D. Dickey, *ACS Appl. Mater. Interfaces*, 2014, DOI: 10.1021/am506496u.
32. D. Kim, D.-W. Lee, W. Choi and J.-B. Lee, J. MEMS, 2013, **22**,1267-1275.
33.G. Li, M. Parmar, D. Kim, J.-B. J. Lee and D.-W. Lee, *Lab Chip*, 2014, **14**, 200-209.
34. J.-H. So and M. D. Dickey, *Lab Chip*, 2011, **11**, 905-911.
35.H. Ota, K. Chen, Y. Lin, D. Kiriya, H. Shiraki, Z. Yu, T.-J. Ha and A. Javey, *Nat Commun*, 2014, **5**.
36.S. P. Maruvada and H. N. Cavallius, *IEEE Trans Power Appar. Sys.*, 1975, **PAS-94**, 1708-1713.
37.A. Chakrabarti, S. Nath and C. K. Chanda, *Basic Electrical Engineering*, McGraw-Hill Education (India) Pvt Limited, 2009.
38.M. Passlack, N. Hunt, E. Schubert, G. Zydzik, M. Hong, J. Mannaerts, R. Opila and R. Fischer, *App. Phys. Lett.*, 1994, **64**, 2715-2717.
39.M. R. Khan, C. B. Eaker, E. F. Bowden and M. D. Dickey, *Proc. Natl. Acad. Sci. U. S. A.*, 2014, **111**, 14047-14051.
40.C. S. Sangeeth, A. Wan and C. A. Nijhuis, *J. Amer. Chem. Soc.*, 2014, **136**, 11134-11144.